Nature of the 1/3 Magnetization Plateau in Spin-1/2 Kagome Antiferromagnets

Li-Wei He[1], Xinzhe Wang[1], Shun-Li Yu[1,2*], and Jian-Xin Li[1,2*]

[1]*National Laboratory of Solid State Microstructures and Department of Physics, Nanjing University, Nanjing 210093, China*
[2]*Collaborative Innovation Center of Advanced Microstructures, Nanjing University, Nanjing 210093, China*

(Received 16 April 2025; accepted manuscript online 15 July 2025)

We investigate the origin of the 1/3 magnetization plateau in the $S = 1/2$ kagome antiferromagnetic Heisenberg model using the variational Monte Carlo and exact diagonalization methods, to account for the recent experimental observations in $YCu_3(OH)_{6+x}Br_{3-x}$ and $YCu_3(OD)_{6+x}Br_{3-x}$. We identify three degenerate valence-bond-solid (VBS) states forming a $\sqrt{3}\times\sqrt{3}$ unit cell. These states exhibit David-star patterns in the spin moment distribution with only two fractional values $-1/3$ and $2/3$, and are related through translational transformations. While the spin correlations in these VBS states are found to be short-range, resembling a quantum spin liquid, we show that they have a vanishing topological entanglement entropy and thus are topologically trivial many-body states. Our theoretical results provide strong evidence that the 1/3 magnetization plateau observed in recent experiments arises from these $\sqrt{3}\times\sqrt{3}$ VBS states with fractional spin moments.

DOI: 10.1088/0256-307X/42/9/090704 CSTR: 32039.14.0256-307X.42.9.090704

1. Introduction. The kagome lattice, a two-dimensional network of corner-sharing triangles arranged in a hexagonal motif [as shown in Fig. 1(a)], has emerged as one of the most versatile platforms in condensed matter physics. Its unique geometry gives rise to a variety of exotic quantum phenomena, including novel quantum magnetism,[1–4] unconventional superconductivity,[5–16] charge density wave orders,[6,9,12,14,17–19] and topological quantum states.[20–27] Of particular interest is its potential to realize quantum spin liquids (QSLs)[28–38] owing to the remarkable combination of strong geometric frustration and a low coordination number. Theoretically, while there is still no consensus on the precise nature of the ground state of the spin-1/2 kagome antiferromagnetic Heisenberg model, many studies suggest that the ground state of the system could be a QSL. On the experimental front, kagome antiferromagnets such as herbertsmithite,[39–42] Zn-barlowite,[43–47] and $YCu_3(OH)_{6+x}Br_{3-x}$[48,49] have shown great promise as QSL candidates.

Recent breakthroughs in kagome magnetism have further highlighted its unique role. In particular, experiments in two kagome antiferromagnets, $YCu_3(OH)_{6+x}Br_{3-x}$ and $YCu_3(OD)_{6+x}Br_{3-x}$,[50–54] have revealed a striking sequence of magnetization plateaus under magnetic fields. At low fields, a 1/9 magnetization plateau phase emerges, while a 1/3 magnetization plateau occurs at higher fields. The 1/9 plateau has been interpreted as either a $\mathbb{Z}_3$ QSL, as suggested by variational Monte Carlo (VMC)[55] and density matrix renormalization group (DMRG) simulations of a $S = 1/2$ kagome antiferromagnet,[56] or a valence-bond-solid (VBS) state, as proposed by tensor network calculations.[57,58] The 1/3 magnetization plateau in the kagome antiferromagnet Heisenberg model has also been found in DMRG simulations[56] and is suggested to originate from a VBS with a configuration where each triangular unit consisting of one fully polarized spin with scaled moment $M_i/M_s = 1$ ($M_s = 1/2$ is the saturated magnetization for spin-1/2 system) and two spins forming a singlet.

In this Letter, we theoretically identify three degenerate VBS states with a unit-cell size of $\sqrt{3}\times\sqrt{3}$ within the 1/3 magnetization plateau phase of a $S = 1/2$ kagome antiferromagnetic Heisenberg model, using the VMC and exact diagonalization (ED) methods. The magnetization distributions of these VBS states differ fundamentally from that proposed in Ref. [56], in that each triangular unit consists of a fractional $M_i/M_s = -1/3$ spin moment and two fractional 2/3 moments. This feature of fractional spin moments demonstrates that the 1/3 magnetization plateau phase contributed by these VBS states cannot be described by semiclassic linear spin-wave theory, which treats the spin as a classic three-dimensional vector. The relevance of the VBS states has been checked by calculating the overlap between their wave functions and those obtained by ED method, and the result shows that the overlap values are $\gtrsim$60% compared to a value 33% for the state envisaged in DMRG simulations.[56] Thus, we ascribe the observed 1/3 magnetization plateau in recent experiments[51–54] to its origin from the VBS states with two fractional moments. We further find that these VBS states exhibit short-range spin–spin correlation, which is quite similar to that in the $\mathbb{Z}_3$ QSL.[55] However, they have zero topological entanglement entropy, indicating a lack of intrinsic topological order which is intrinsically different from a gapped QSL.

*Corresponding authors. Email: slyu@nju.edu.cn; jxli@nju.edu.cn
© 2025 Chinese Physical Society and IOP Publishing Ltd. All rights, including for text and data mining, AI training, and similar technologies, are reserved.

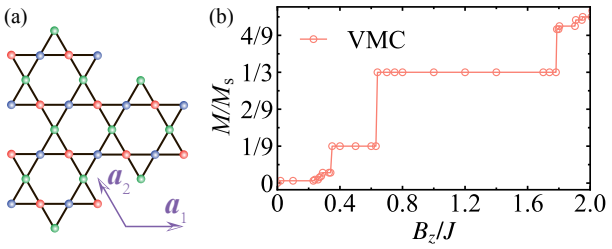

Fig. 1. (a) Kagome lattice. The three different colors represent the three sublattices. The purple arrows indicate the basis vectors $\boldsymbol{a}_1 = (1, 0)$ and $\boldsymbol{a}_2 = (-1/2, \sqrt{3}/2)$ of its primitive cell. (b) The average magnetization M/M_s as a function of the magnetic field B_z/J, obtained using the VMC method for a large system with at least $N = 12 \times 12 \times 3 = 432$ sites.

2. Model and Method. The Hamiltonian of the spin-1/2 kagome antiferromagnet with a magnetic field is given by

$$H = J \sum_{\langle ij \rangle} \boldsymbol{S}_i \cdot \boldsymbol{S}_j - B_z \sum_i S_i^z, \tag{1}$$

where $\langle ij \rangle$ denotes the sum over nearest-neighbor (NN) bonds, $\boldsymbol{S}_i$ represents the spin-1/2 operator at site i (with S_i^z representing its z-component), J is the exchange interaction, and B_z is the magnitude of the external magnetic field. For finite B_z, the total S^z remains conserved.

In the standard VMC process, we introduce the fermionic doublet to represent the spin operator, $S_i^\alpha = \frac{1}{2}\psi_i^\dagger \sigma_\alpha \psi_i$, where $\alpha \in \{x, y, z\}$, $\psi = (c_{i\uparrow}, c_{i\downarrow})^{\mathrm{T}}$ and $c_{i\uparrow(\downarrow)}$ are the annihilation operators of the spin-up (down) spinons, respectively, and σ_α are the Pauli matrices. For spin-1/2 system, the single-occupancy constrain $N_i = n_{i\uparrow} + n_{i\downarrow} = \psi_i^\dagger \psi_i = 1$ is necessary. We then decouple the model (1) into its non-interacting mean-field form using the above representation,

$$H_{\mathrm{mf}} = \sum_{\langle ij \rangle} t_{ij} \psi_i^\dagger \psi_j + \mathrm{h.c.} - \mu \sum_i \psi_i^\dagger \sigma_z \psi_i, \tag{2}$$

where t_{ij} are the spinon hopping terms between the NN site i and j, μ is the chemical potential modulated by the field B_z and determines the magnetization. The system size used in the VMC method is always finite, and the magnetization should increase gradually in the form of steps with the field for a system that conserves total S^z conservation. The ground state of H_{mf} can be denoted as $|\mathrm{GS}(t_{ij})_{\mathrm{mf}}\rangle$ as a function of the hopping parameters t_{ij}. After applying the Gutzwiller projection $P_{\mathrm{G}} = \prod_i (1 - n_{i\uparrow} n_{i\downarrow})$, the many-body trial wave function is obtained as $|\Psi(t_{ij})\rangle = P_{\mathrm{G}} |\mathrm{GS}(t_{ij})_{\mathrm{mf}}\rangle$. The t_{ij} parameters are treated as variational parameters in the VMC calculation and are determined by minimizing the expectation value $E(t_{ij}) = \langle \Psi(t_{ij}) | H | \Psi(t_{ij}) \rangle / \langle \Psi(t_{ij}) | \Psi(t_{ij}) \rangle$. Our main results are obtained for a system with $L_{1,2} = 12$, which are the lengths along the basis vectors $\boldsymbol{a}_{1,2}$ as shown in Fig. 1(a), unless otherwise stated.

3. Results. As shown in Fig. 1(b), broad 1/9- and 1/3-magnetization plateau phases are identified using the VMC method, aligning qualitatively with experimental

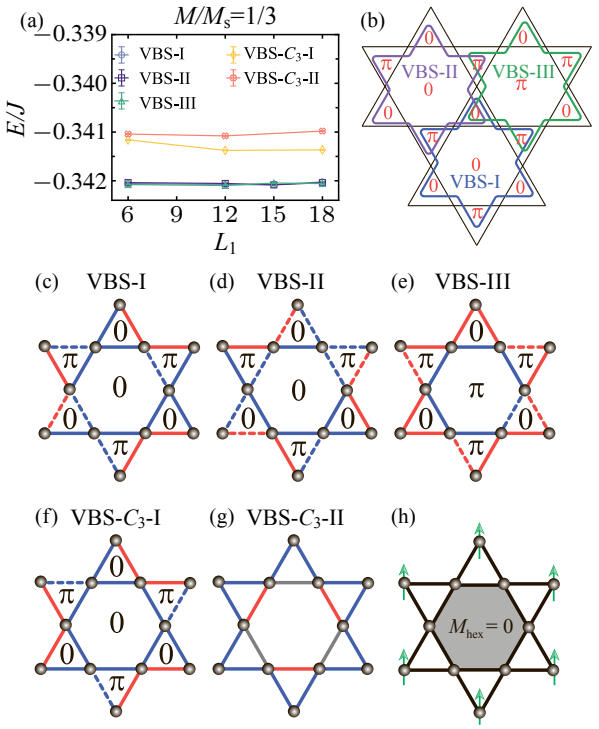

Fig. 2. (a) Variational energies per site (excluding the contribution $E(B_z) = -B_z/6$ from the magnetic field) for several VBS states with 1/3 magnetization are shown as a function of the length L_1 along vector $\boldsymbol{a}_1$ for system sizes of $L_1 \times 12 \times 3$. (b) Illustration of spatial $\mathbb{Z}_3$-cyclic domain adjacency consisting of the "VBS-I","VBS-II" and "VBS-III" states. (c)–(g) The unit-cell patterns of the "VBS-I","VBS-II", "VBS-III", "VBS-C_3-I" and "VBS-C_3-II" states. Solid (dashed) bonds indicate positive (negative) signs of the spinon hoppings, while red and blue bonds represent different hopping magnitudes. The gray bonds in (g) indicate vanishing hopping terms. (h) The magnetization pattern of the VBS state proposed for the 1/3 magnetization plateau in Ref. [56]. The green arrows represent fully polarized spins, and the magnetization of the shaded hexagon is zero.

observations[51–54] and theoretical results.[55–58] Given the detailed previous VMC studies on the 1/9 magnetization plateau phase,[55] we focus here on the 1/3 magnetization plateau phase. The magnetic field range for the 1/3 plateau is $0.64 \lesssim B_z/J \lesssim 1.79$, slightly broader than that obtained via DMRG calculations[56] due to the difficulty in precisely capturing intermediate states with the VMC method. For the 1/3-magnetization plateau, we identify three energetically favorable VBS states as potential ground states, which are degenerate within numerical error, as shown in Fig. 2(a). Furthermore, the overlaps between them are zero, indicating that these VBS states are orthogonal and distinctly different. Their unit cells are three times larger than the primitive cell of the kagome lattice, comprising nine sublattices. These states represent three different domains in the VBS phase [see Fig. 2(b)] and can be mapped to the state space of the $\mathbb{Z}_3$ clock model,[59–62] characterized by the global $\mathbb{Z}_3$ symmetry structure. Each VBS configuration corresponds to a distinct spontaneously broken pattern of the $\mathbb{Z}_3$ symmetry. In the VMC process, we can fix one of the hoppings to be 1 as a reference; then, there are 17 independent hopping terms.

Due to large variational parameter space, we perform repeated VMC calculations starting from various initial parameters. Ultimately, we identify three VBS states with hopping patterns displayed in Figs. 2(c)–2(e), respectively; where gauge fluxes and the magnitudes of two types of hopping terms maintain C_3 rotational symmetry. However, if we artificially adjust positions of hopping terms with negative signs while keeping the flux pattern unchanged to give rise to David-star C_3 rotational symmetry, this artificial VBS state shown in Fig. 2(f) is not energetically favorable as seen in Fig. 2(a). Additionally, the energy per site of "VBS-C_3-Ⅱ" state named in Fig. 2(a) is the highest; its hopping pattern is derived from previous work [55] featuring a $2\pi/3$ flux through each primitive cell of the kagome lattice due to complex hopping terms. We find optimal gauge fluxes are zero (mod 2π) in all minimal triangles, with nearly vanishing three hopping terms. By eliminating phases of these hopping terms, we find this artificial state is equivalent to the unmodified one. Therefore, we present the reduced hopping pattern with C_3 rotational symmetry, as shown in Fig. 2(g).

As a benchmark, we perform an ED calculation on a small cluster with $N = 3 \times 3 \times 3 = 27$, which is the upper limit of our computational capacity. We then calculate the maximal overlaps between the ground state obtained by the ED method and the VBS-I, -Ⅱ and -Ⅲ states, as listed in Table 1. These states share a significant weight ($\gtrsim$60%) of the ED ground states, with minimal differences among the three VBS states. Additionally, we also examine the 1/3-plateau VBS state as defined in Ref. [56], where the spins at the six vertices of the David star are fully polarized to 1/2, while the magnetization of the internal hexagon remains zero, as illustrated in Fig. 2(h). For the sake of simplicity, we refer to this state as the "VBS-Ref" state. According to this definition, the representation of the "VBS-Ref" state in the $3 \times 3 \times 3$ cluster is given by

$$|\Psi_{\mathrm{Ref}}\rangle = \prod_{i=1}^{N_{\mathrm{star}}} |\phi_i\rangle \prod_{j\in \mathrm{vertex}} |\uparrow_j\rangle, \tag{3}$$

where $N_{\mathrm{star}} = 3$ is the number of David stars in this cluster, $|\phi_i\rangle$ represents the ground state of the hexagon with total $S^z = 0$ in the i-th David star, solved using the ED method, and $|\uparrow_j\rangle$ denotes the fully polarized spin state at site j. We then calculate the maximal overlap $|\langle\Psi_{\mathrm{Ref}}|\Psi_{\mathrm{ED}}\rangle|^2$ and list it in the last column in Table 1. This value is nearly half as small as those of the three VBS states obtained from the VMC calculations. Based on the ED method benchmark, we believe our VMC results are sufficiently reliable.

Furthermore, we examine the magnetization distributions of the three degenerate VBS states, depicted in Figs. 3(a)–3(c), respectively. Remarkably, the magnetization moments exhibit fractional values $M_i/M_s = -1/3$ and 2/3 within numerical error. To our knowledge, we do not find the similar example of a magnetic structure with fraction moments in a VBS state responsible for 1/3 magnetization plateau discussed before. Additionally, the magnetization patterns form a David-star shape and

Table 1. Overlaps $\mathcal{O} = |\langle \mathrm{VBS}|\Psi_{\mathrm{ED}}\rangle|^2$, where $|\mathrm{VBS}\rangle$ denotes the wave functions of VBS-I, -Ⅱ, -Ⅲ states and the VBS-Ref state proposed in Ref. [56], respectively, and $|\Psi_{\mathrm{ED}}\rangle$ is the ground-state wave function obtained by ED method in the cluster with $3 \times 3 \times 3 = 27$ sites. We note the optimal variational parameters in the VBS-I, -Ⅱ and -Ⅲ states from the system with $12 \times 12 \times 3$ sites.

State	VBS-I	VBS-Ⅱ	VBS-Ⅲ	VBS-Ref
$\mathcal{O}$	0.5946	0.6880	0.5934	0.3335

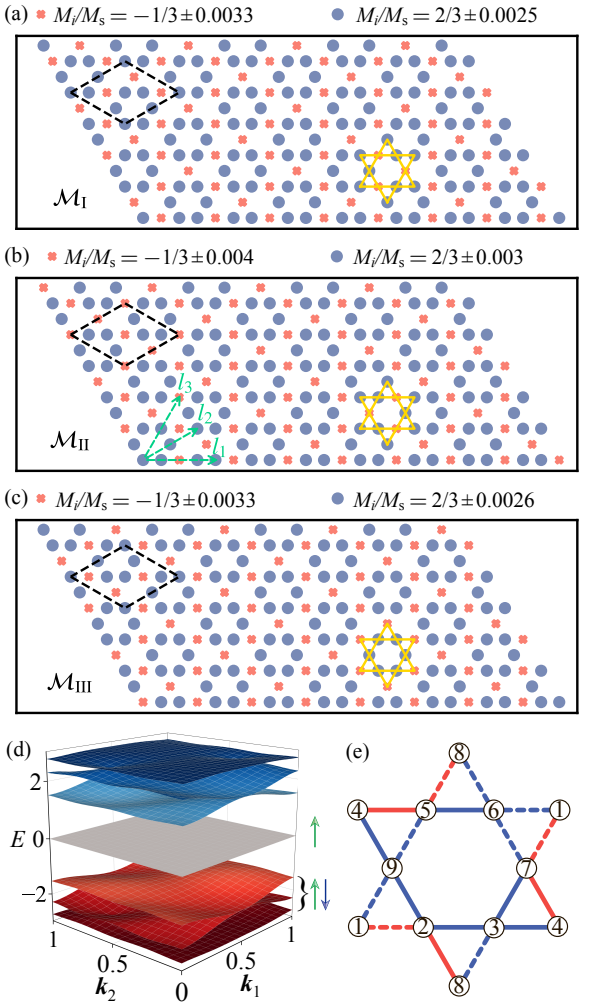

Fig. 3. (a)–(c) The magnetization distributions $\mathcal{M}_{\mathrm{I}}$, $\mathcal{M}_{\mathrm{II}}$ and $\mathcal{M}_{\mathrm{III}}$ for the VBS-I,-Ⅱ and -Ⅲ states, respectively. The dashed black lines denote the $\sqrt{3} \times \sqrt{3}$ unit cells for these three states, while the solid yellow lines mark the corresponding positions of the David stars formed by hopping patterns, as shown in Figs. 2(c)–2(e). (d) The spinon dispersion derived from the Ansätz of VBS-Ⅱ state with optimal variational parameters in the $120 \times 120 \times 9$ system, where $\boldsymbol{k}_1 = (3/2, \sqrt{3}/2)$ and $\boldsymbol{k}_2 = (-3/2, \sqrt{3}/2)$ are the reciprocal vectors. The flat band with $E = 0$ is threefold degenerate. (e) The indices of 9 sublattices in the VBS-Ⅱ state.

are related by the translational transformations $T_{1,2}$, such as $\mathcal{M}_{\mathrm{III}} \xrightarrow{T_1} \mathcal{M}_{\mathrm{II}} \xrightarrow{T_1} \mathcal{M}_{\mathrm{I}}$. The magnetization distributions obtained from the VMC calculations here differ significantly from that proposed in Ref. [56], despite all of them exhibit David-star structures. Moreover, one can notice that the C_3 rotational symmetry of the magnetization

distributions for the three VBS states are preserved.

Though the fractional spin moment distribution is believed to originate from strong quantum fluctuations, we may still get some useful information from the spinon dispersion. Figure 3(d) shows the spinon dispersion of the VBS-Ⅱ state, which has the largest overlap with the wave function $|\Psi_{\rm ED}\rangle$, as listed in Table 1. There are nine bands in total, where the spin-up (spin-down) spinons occupy six (three) bands accounting for the 1/3 magnetization. Notably, the spin-up spinons occupy three degenerate flat bands, which apply to all three degenerate VBS states. To determine the contribution per site of the three flat bands, we define a weight factor as follows:

$$f_\alpha = \sum_{n,\boldsymbol{k}} |\langle 0|c_{\alpha\uparrow}\gamma^\dagger_{n,\boldsymbol{k}}|0\rangle|, \tag{4}$$

where $|0\rangle$ is the vacuum, α is the index of the sublattice as shown in Fig. 3(e), $\gamma^\dagger_{n,\boldsymbol{k}}$ is the creation operator of the mean-field quasi-particle with momentum $\boldsymbol{k}$ for the n-th flat band. We find two different weight factors: $f_{1,2,4,5,7,8} = 0.39377$ and $f_{3,6,9} = 0.21246$, indicating that the magnetization per site should take these values at the corresponding sublattices. Thus, the three flat bands are related to all nine sublattices rather than just any three, and the magnetic moment distribution structure is consistent with VMC calculations, disregarding the sign of the magnetic moment. Of course, the detailed distribution of magnetization is significantly influenced by many-body correlation effects, which deserve further investigation. We note that a similar argument applies to the VBS-I and -Ⅲ states.

For the 1/3-magnetization plateau phase, the number of the sites in a unit cell is $n = 9$. Consequently, the relationship $n(S - M) = \frac{9}{2}(1 - \frac{1}{3}) = 3$ being an integer, aligns with the theory of magnetization plateaus.[56,63,64] This implies all three VBS states have no $\mathbb{Z}_q (q \geq 2)$ gauge structure. Conversely, for the $\mathbb{Z}_3$ QSL state at the 1/9-magnetization plateau,[55,56] $n(S - M) = \frac{3}{2}(1 - \frac{1}{9}) = 4/3$ due to the $\mathbb{Z}_3$ gauge field as mentioned in Ref. [64]. These results suggest that the denominator of $n(S-M)$ is closely related to the gauge structure of the many-body quantum state. This is an intriguing issue that warrants further study.

With the introduction of the finite field B_z, the system reduces the $SU(2)$ symmetry to $U(1)$, resulting in the transverse and longitudinal components of the spin correlation becoming non-equivalent. As shown in Fig. 4(a), we calculate all three components of the spin correlation $C(r)$ as a function of the distance r between two sites along three different directions for the VBS-Ⅱ state. The x- and y-components are identical, differing from the z-component, which is consistent with $U(1)$ symmetry. Although the results indicate that the spin correlation is entirely short-range, similar to a QSL state, the topological entanglement entropy is nearly zero within numerical error, as shown in Fig. 4(b). This suggests that the VBS state lacks long-range entanglement and is topologically trivial according to the classification of topological order.[65,66]

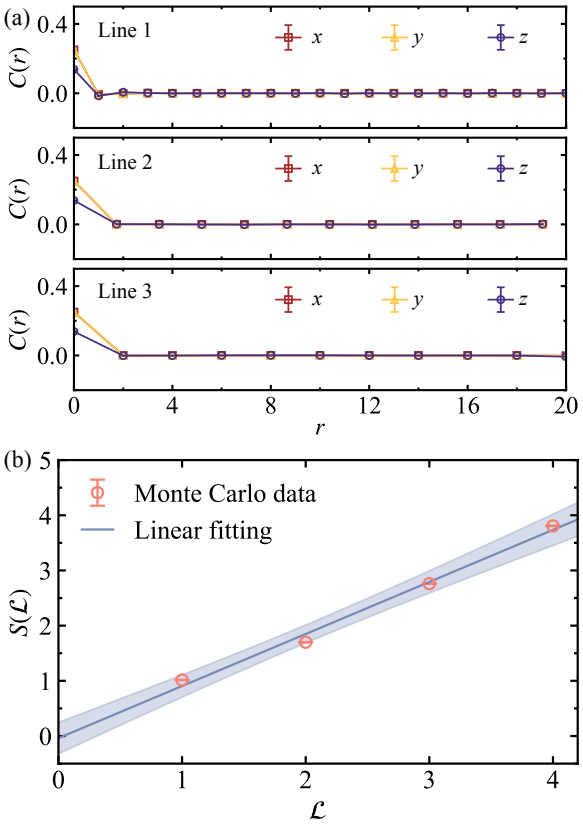

Fig. 4. (a) Spin correlation $C(r)$ as a function of distance r along the three green dashed lines in Fig. 3(b), labeled with arrows $l_{1,2,3}$. The legend $\alpha \in \{x, y, z\}$ denotes the α-component correlation $C(r) = \langle S^\alpha_0 S^\alpha_r\rangle - \langle S^\alpha_0\rangle\langle S^\alpha_r\rangle$. (b) Entropy of the VBS-Ⅱ state for a system size of $L_{1,2} = 12$. The best linear fit, $S(\mathcal{L}) = \alpha\mathcal{L} - \gamma$, yields a topological entanglement entropy $\gamma \approx 0.038 \pm 0.286$, where $\mathcal{L}$ represents the area of the subsystem as $\mathcal{L}^2\boldsymbol{a}_1 \cdot \boldsymbol{a}_2$. The blue shading indicates the confidence interval for the linear fitting.

4. Conclusions. In summary, we elaborate that the ground state of the 1/3 magnetization plateau phase in the spin-1/2 kagome antiferromagnetic Heisenberg model exhibits a triply degenerate $\sqrt{3}\times\sqrt{3}$ VBS order, as revealed through VMC and ED methods. These VBS states exhibit fractional spin moments, which differ significantly from those previously proposed using the DMRG method,[56] where fully polarized spin moments exist. Additionally, while the spin correlations in these VBS states are short-range, similar to QSL states, they are topologically trivial, as indicated by the vanishing topological entanglement entropy.

Acknowledgements. This work was supported by the National Key Projects for Research and Development of China (Grant Nos. 2021YFA1400400 and 2024YFA1408104) and the National Natural Science Foundation of China (Grant Nos. 12434005, 12374137, and 92165205).

References

[1] Zorko A, Nellutla S, van Tol J, Brunel L C, Bert F, Duc F, Trombe J C, de Vries M A, Harrison A, and Mendels P 2008 *Phys. Rev. Lett.* **101** 026405

[2] Matan K, Bartlett B M, Helton J S, Sikolenko V, Mat'aš S, Prokeš K, Chen Y, Lynn J W, Grohol D, Sato T J, Tokunaga M, Nocera D G, and Lee Y S 2011 *Phys. Rev. B* **83** 214406

[3] Ye L, Kang M, Liu J, von Cube F, Wicker C R, Suzuki T, Jozwiak C, Bostwick A, Rotenberg E, Bell D C, Fu L, Comin R, and Checkelsky J G 2018 *Nature* **555** 638

[4] Yin J X, Zhang S S, Li H, Jiang K, Chang G, Zhang B, Lian B, Xiang C, Belopolski I, Zheng H, Cochran T A, Xu S Y, Bian G, Liu K, Chang T R, Lin H, Lu Z Y, Wang Z, Jia S, Wang W, and Hasan M Z 2018 *Nature* **562** 91

[5] Ko W H, Lee P A, and Wen X G 2009 *Phys. Rev. B* **79** 214502

[6] Yu S L and Li J X 2012 *Phys. Rev. B* **85** 144402

[7] Ortiz B R, Teicher S M L, Hu Y, Zuo J L, Sarte P M, Schueller E C, Abeykoon A M M, Krogstad M J, Rosenkranz S, Osborn R, Seshadri R, Balents L, He J, and Wilson S D 2020 *Phys. Rev. Lett.* **125** 247002

[8] Chen H, Yang H, Hu B, Zhao Z, Yuan J, Xing Y, Qian G, Huang Z, Li G, Ye Y, Ma S, Ni S, Zhang H, Yin Q, Gong C, Tu Z, Lei H, Tan H, Zhou S, Shen C, Dong X, Yan B, Wang Z, and Gao H J 2021 *Nature* **599** 222

[9] Neupert T, Denner M M, Yin J X, Thomale R, and Hasan M Z 2022 *Nat. Phys.* **18** 137

[10] Chen H, Hu B, Ye Y, Yang H, and Gao H J 2022 *Chin. Phys. B* **31** 097405

[11] Yin J X, Lian B, and Hasan M Z 2022 *Nature* **612** 647

[12] Nie L, Sun K, Ma W, Song D, Zheng L, Liang Z, Wu P, Yu F, Li J, Shan M, Zhao D, Li S, Kang B, Wu Z, Zhou Y, Liu K, Xiang Z, Ying J, Wang Z, Wu T, and Chen X 2022 *Nature* **604** 59

[13] Jiang K, Wu T, Yin J X, Wang Z, Hasan M Z, Wilson S D, Chen X, and Hu J 2022 *Natl. Sci. Rev.* **10** nwac199

[14] Wang Y, Wu H, McCandless G T, Chan J Y, and Ali M N 2023 *Nat. Rev. Phys.* **5** 635

[15] Wilson S D and Ortiz B R 2024 *Nat. Rev. Mat.* **9** 420

[16] You J Y, Hsu C E, Del Ben M, and Li Z 2025 *Phys. Rev. Lett.* **134** 106401

[17] Zheng L, Wu Z, Yang Y, Nie L, Shan M, Sun K, Song D, Yu F, Li J, Zhao D, Li S, Kang B, Zhou Y, Liu K, Xiang Z, Ying J, Wang Z, Wu T, and Chen X 2022 *Nature* **611** 682

[18] Yi S, Liao Z, Wang Q, Ma H, Liu J, Teng X, Gao B, Dai P, Dai Y, Zhao J, Qi Y, Xu B, and Qiu X 2025 *Phys. Rev. Lett.* **134** 086902

[19] Elmers H J, Tkach O, Lytvynenko Y, Yogi P, Schmitt M, Biswas D, Liu J, Chernov S V, Nguyen Q, Hoesch M, Kutnyakhov D, Wind N, Wenthaus L, Scholz M, Rossnagel K, Gloskovskii A, Schlueter C, Winkelmann A, Haghighirad A A, Lee T L, Sing M, Claessen R, Le Tacon M, Demsar J, Schönhense G, and Fedchenko O 2025 *Phys. Rev. Lett.* **134** 096401

[20] Guo H M and Franz M 2009 *Phys. Rev. B* **80** 113102

[21] Yu S L, Li J X, and Sheng L 2009 *Phys. Rev. B* **80** 193304

[22] Wen J, Rüegg A, Wang C C J, and Fiete G A 2010 *Phys. Rev. B* **82** 075125

[23] Xu G, Lian B, and Zhang S C 2015 *Phys. Rev. Lett.* **115** 186802

[24] O'Brien A, Pollmann F, and Fulde P 2010 *Phys. Rev. B* **81** 235115

[25] Tang E, Mei J W, and Wen X G 2011 *Phys. Rev. Lett.* **106** 236802

[26] Rüegg A and Fiete G A 2011 *Phys. Rev. B* **83** 165118

[27] Liu D F, Liang A J, Liu E K, Xu Q N, Li Y W, Chen C, Pei D, Shi W J, Mo S K, Dudin P, Kim T, Cacho C, Li G, Sun Y, Yang L X, Liu Z K, Parkin S S P, Felser C, and Chen Y L 2019 *Science* **365** 1282

[28] Ran Y, Hermele M, Lee P A, and Wen X G 2007 *Phys. Rev. Lett.* **98** 117205

[29] Jiang H C, Weng Z Y, and Sheng D N 2008 *Phys. Rev. Lett.* **101** 117203

[30] Yan S, Huse D A, and White S R 2011 *Science* **332** 1173

[31] Depenbrock S, McCulloch I P, and Schollwöck U 2012 *Phys. Rev. Lett.* **109** 067201

[32] Iqbal Y, Becca F, Sorella S, and Poilblanc D 2013 *Phys. Rev. B* **87** 060405

[33] Liao H J, Xie Z Y, Chen J, Liu Z Y, Xie H D, Huang R Z, Normand B, and Xiang T 2017 *Phys. Rev. Lett.* **118** 137202

[34] He Y C, Zaletel M P, Oshikawa M, and Pollmann F 2017 *Phys. Rev. X* **7** 031020

[35] Mei J W, Chen J Y, He H, and Wen X G 2017 *Phys. Rev. B* **95** 235107

[36] Chen X, Ran S J, Liu T, Peng C, Huang Y Z, and Su G 2018 *Sci. Bull.* **63** 1545

[37] Zhu W, Chen X, He Y C, and Witczak-Krempa W 2018 *Sci. Adv.* **4** eaat5535

[38] He L W and Li J X 2024 *Phys. Rev. B* **110** 035131

[39] Helton J S, Matan K, Shores M P, Nytko E A, Bartlett B M, Yoshida Y, Takano Y, Suslov A, Qiu Y, Chung J H, Nocera D G, and Lee Y S 2007 *Phys. Rev. Lett.* **98** 107204

[40] Han T H, Helton J S, Chu S, Nocera D G, Rodriguez-Rivera J A, Broholm C, and Lee Y S 2012 *Nature* **492** 406

[41] Fu M, Imai T, Han T H, and Lee Y S 2015 *Science* **350** 655

[42] Khuntia P, Velazquez M, Barthélemy Q, Bert F, Kermarrec E, Legros A, Bernu B, Messio L, Zorko A, and Mendels P 2020 *Nat. Phys.* **16** 469

[43] Feng Z, Li Z, Meng X, Yi W, Wei Y, Zhang J, Wang Y C, Jiang W, Liu Z, Li S, Liu F, Luo J, Li S, Zheng G Q, Meng Z Y, Mei J W, and Shi Y 2017 *Chin. Phys. Lett.* **34** 077502

[44] Feng Z, Wei Y, Liu R, Yan D, Wang Y C, Luo J, Senyshyn A, Cruz C D, Yi W, Mei J W, Meng Z Y, Shi Y, and Li S 2018 *Phys. Rev. B* **98** 155127

[45] Wei Y, Ma X, Feng Z, Adroja D, Hillier A, Biswas P, Senyshyn A, Hoser A, Mei J W, Meng Z Y, Luo H, Shi Y, and Li S 2020 *Chin. Phys. Lett.* **37** 107503

[46] Tustain K, Ward-O'Brien B, Bert F, Han T, Luetkens H, Lancaster T, Huddart B M, Baker P J, and Clark L 2020 *npj Quantum Mater.* **5** 74

[47] Fu Y, Lin M L, Wang L, Liu Q, Huang L, Jiang W, Hao Z, Liu C, Zhang H, Shi X, Zhang J, Dai J, Yu D, Ye F, Lee P A, Tan P H, and Mei J W 2021 *Nat. Commun.* **12** 3048

[48] Zeng Z, Ma X, Wu S, Li H F, Tao Z, Lu X, Chen X H, Mi J X, Song S J, Cao G H, Che G, Li K, Li G, Luo H, Meng Z Y, and Li S 2022 *Phys. Rev. B* **105** L121109

[49] Xu A, Shen Q, Liu B, Zeng Z, Han L, Yan L, Luo J, Yang J, Zhou R, and Li S 2024 *Phys. Rev. B* **110** 085146

[50] Zeng Z, Zhou C, Zhou H, Han L, Chi R, Li K, Kofu M, Nakajima K, Wei Y, Zhang W, Mazzone D G, Meng Z Y, and Li S 2024 *Nat. Phys.* **20** 1097

[51] Jeon S, Wulferding D, Choi Y, Lee S, Nam K, Kim K H, Lee M, Jang T H, Park J H, Lee S, Choi S, Lee C, Nojiri H, and Choi K Y 2024 *Nat. Phys.* **20** 435

[52] Suetsugu S, Asaba T, Kasahara Y, Kohsaka Y, Totsuka K, Li B, Zhao Y, Li Y, Tokunaga M, and Matsuda Y 2024 *Phys. Rev. Lett.* **132** 226701

[53] Zheng G, Zhang D, Zhu Y, Chen K W, Chan A, Jenkins K, Kang B, Zeng Z, Xu A, Ratkovski D, Blawat J, Bangura A F, Singleton J, Lee P A, Li S, and Li L 2025 *Phys. Rev. X* **15** 021076

[54] Zheng G, Zhu Y, Chen K W, Kang B, Zhang D, Jenkins K, Chan A, Zeng Z, Xu A, Valenzuela O A, Blawat J, Singleton J, Li S, Lee P A, and Li L 2025 *Proc. Natl. Acad. Sci.* **122** e2421390122

[55] He L W, Yu S L, and Li J X 2024 *Phys. Rev. Lett.* **133** 096501

[56] Nishimoto S, Shibata N, and Hotta C 2013 *Nat. Commun.* **4** 2287
[57] Picot T, Ziegler M, Orús, and Poilblanc D 2016 *Phys. Rev. B* **93** 060407
[58] Fang D Z, Xi N, Ran S J, and Su G 2023 *Phys. Rev. B* **107** L220401
[59] Vishwanath A, Balents L, and Senthil T 2004 *Phys. Rev. B* **69** 224416
[60] Sun G, Vekua T, Cobanera E, and Ortiz G 2019 *Phys. Rev. B* **100** 094428
[61] Goswami A, Kumar R, Gope M, and Sahoo S 2025 *Phys. Rev. E* **111** 054125
[62] Butt N, Jin X Y, Osborn J C, and Saleem Z H 2023 *Phys. Rev. D* **108** 074511
[63] Oshikawa M, Yamanaka M, and Affleck I 1997 *Phys. Rev. Lett.* **78** 1984
[64] Tanaka A, Totsuka K, and Hu X 2009 *Phys. Rev. B* **79** 064412
[65] Wen X G 2015 *Natl. Sci. Rev.* **3** 68
[66] Wen X G 2017 *Rev. Mod. Phys.* **89** 041004